A model of flow and surfactant transport in an oscillatory alveolus partially filled with liquid

Hsien-Hung Wei[a] and Hideki Fujioka
Biomedical Engineering Department, University of Michigan, Ann Arbor, Michigan 48109

Ronald B. Hirschl
Department of Surgery, University of Michigan, Ann Arbor, Michigan 48109

James B. Grotberg
Biomedical Engineering Department, University of Michigan, Ann Arbor, Michigan 48109

(Received 26 June 2003; accepted 24 November 2003; published online 1 March 2005)

The flow and transport in an alveolus are of fundamental importance to partial liquid ventilation, surfactant transport, pulmonary drug administration, cell-cell signaling pathways, and gene therapy. We model the system in which an alveolus is partially filled with liquid in the presence of surfactants. By assuming a circular interface due to sufficiently strong surface tension and small surfactant activity, we combine semianalytical and numerical techniques to solve the Stokes flow and the surfactant transport equations. In the absence of surfactants, there is no steady streaming because of reversibility of Stokes flow. The presence of surfactants, however, induces a nontrivial cycle-averaged surfactant concentration gradient along the interface that generates steady streaming. The steady streaming patterns (e.g., number of vortices) particularly depend on the ratio of inspiration to expiration periods ($I:E$ ratio) and the sorption parameter K. For an insoluble surfactant, a single vortex is formed when the $I:E$ ratio is either smaller or larger than 1:1, but the recirculations have opposite directions in the two cases. A soluble surfactant can lead to more complex flow patterns such as three vortices or saddle-point flow structures. The estimated unsteady velocity is 10^{-3} cm/s, and the corresponding Péclet number for transporting respiratory gas is $O(1)$. For a cell-cell signaling molecule such as surfactant-associated protein-A for regulating surfactant secretion, the Péclet number could be $O(10)$ or higher. Convection is either comparable to or more dominant than diffusion in these processes. The estimated steady velocity ranges from 10^{-6} to 10^{-4} cm/s, depending on $I:E$ and K, and the corresponding steady Péclet number is between $10^{-8}/D_m$ and $10^{-6}/D_m$ (D_m is the molecular diffusivity with units of cm^2/s). Therefore, for $D_m \leqslant 10^{-8}$ cm^2/s, the convective transport dominates. © *2005 American Institute of Physics*.
[DOI: 10.1063/1.1830487]

I. INTRODUCTION

Alveoli are the major units responsible for gas exchange in the lung. A normal lung produces surfactants to reduce surface tension in the alveolus, making the lung more compliant to aid in breathing. The typical diameter of an alveolus is 250 μm. In a normal lung a liquid layer of average thickness 0.1 μm coats the interior of the alveolus.[1] The transport of oxygen and carbon dioxide in the alveolar gas is dominated by diffusion. However, for respiratory diseases or disorders due to Acute Respiratory Distress Syndrome (ARDS) or the lung injury, alveoli often collapse or are damaged. The remedy often involves surfactant replacement therapy (SRT) or partial liquid ventilation (PLV). In the former, liquid is either instilled into the airways in the form of boluses to deliver macromolecules or clinical agents into the lung; in the latter, a liquid with high gas solubility (e.g., PFC) is used for expanding those shrunken alveoli in order to improve compliance and gas exchange in the lung. In these clinical applications, when such liquid reaches the respiratory bronchioles or alveolar levels, it may partially fill the alveolus and act as a diffusion barrier to transport. Therefore the convection due to alveolar breathing motions may play an important role in determining molecular transport within the alveolus. In addition, alveolar motions could cause a nonuniform interfacial surfactant distribution, generating a surface tension gradient force (Marangoni effect) that modifies the convective processes within the alveolar liquid layer. Thus the presence of surfactant in liquid-filled lungs influences not only the lung compliance, but also the details of the transport processes within alveoli. It is therefore important to address the issues of surfactant transport and its effects on convective processes within alveoli in order to gain further understanding of transport mechanisms in fluid-filled lungs.

Thin-layer flows in an alveolus often occur in a normal lung. Podgorski and Gradon[2] investigated the mechanism of flow clearance due to the presence of surfactant in an alveolus. Their analysis focused on the type "B" alveolus that are directly connected to airways (see Fig. 1). They showed, using lubrication theory, that there is a net flow pumping from the less stiff end (centerline of the alveolus) to the

[a]Author to whom correspondence should be addressed. Present address: Department of Chemical Engineering, National Cheng Kung University, Tainan 701, Taiwan.

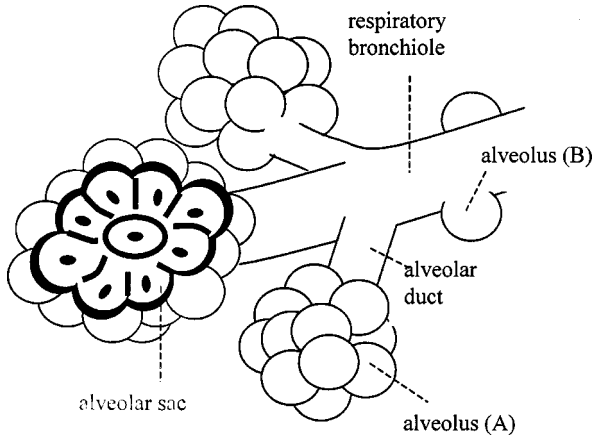

FIG. 1. Respiratory bronchiole and alveoli. The alveolus "A" is in a cluster of alveoli. The alveolus "B" is directly attached to airway.

stiffer end (the alveolar opening) of the alveolar wall. That is, the net flow tends to be pumped out of the alveolus. This is a result of an imbalance of flow pumping out during expiration and pumping in during inspiration. Similar features are also seen in the studies for clearance flow in small airways.[3] However, without additional mass sources, the study by Podgorski and Gradon leads to inevitable losses of fluid and surfactant within an alveolus. Zelig and Haber[4] accounted for additional mass sources to regulate the leakage of fluid and surfactant in the type B alveolus by considering the effects of permeable alveolar walls and the production of natural surfactant. Even though all of these previous studies have accounted for the interfacial deformation, the surface tension force was excluded. That is, they only considered the interplay between the wall stretching motions and the Marangoni effect. The latter is the major mechanism responsible for clearance processes.

However, the role of surface tension in determining alveolar flow may not be simply negligible, particularly for respiratory diseases, e.g., ARDS due to surfactant deficiency. For normal respiratory rate of 12 times/min, a typical capillary number Ca ranges from 10^{-5} to 10^{-4} for surface tensions from 10 to 1 dyne/cm. The resulting capillary pressure arising from the interfacial deformation is so substantial that it is not only comparable to the viscous force due to very thin fluid layer, but also competes with the existing Marangoni force. It is thus necessary to incorporate the surface tension force into the alveolar flow analysis, particularly for respiratory diseases due to the deficiency of surfactant.

Wei *et al.*[5] included the effect of surface tension on the flow and transport of alveolar liquid lining. In addition, they first pointed out the distinction between different types of alveoli in a viewpoint of physiology. That is, the types of alveoli are distinguished by if they are influenced by the airway-alveolar proximity. Their analysis focused on the type "A" alveolus that is not directly connected to an airway, but is found in a cluster of alveoli (see Fig. 1). In contrast to type B alveoli, flow and transport is not possible between adjacent type A alveoli since it can lead to the formation of "dry spots" which are physiologically less plausible in the context of no new sources of lining fluid. This study found that strong surface tension forces can weaken flow clearance processes. The cycle-averaged streamlines exhibited different patterns, depending on surface tension and solubility of surfactant. In the limit of low surface tension, their study captured similar qualitative flow features or tendency as the previous study.[2]

In application such as PLV the fluid thickness may be comparable to the size of an alveolus. This leads to fundamental differences compared to the thin-layer case. First, for a small Ca, capillary force dominates throughout the fluid layer. When the variation of surface tension due to surfactant is small (i.e., a small surfactant activity), the interface shape satisfies the Young–Laplace equation. In contrast to the thin-layer problems where interfacial displacements are comparable to the fluid thickness and strongly couple with the flow field, a small deformation of the interface from its equilibrium shape only induces a correction to the flow field of the thick-layer problem. Second, the surfactant transport for the thick-layer problem may have different dominant mechanisms compared to the thin-layer problem. In the thin-layer problem the surfactant transport is dominated by surface convection. In the thick-layer problem, the change in the local surface area due to expansion/compression can compete with surface convection. Therefore surfactant transport in the thick-layer problem may share features similar to surfactant-laden bubble formation.[6] Finally, for gas transport within an alveolus, the fundamental difference between the thin-layer and the thick-layer problems becomes even more pronounced. For an alveolus with a thin layer as in a normal lung, it is entirely filled with air; air flow apparently has no impact on the gas transport since the Péclet number Pe is small $[O(10^{-3})]$. For a liquid-filled alveolus, however, the estimated Pe could be $O(10)$ or larger, revealing the importance of convection to the gas transport. More importantly, PLV sometimes also serves a means to deliver pulmonary drugs or genes that often exhibit surface-active characteristics. The Marangoni effects induced by surface-active agents can modify the detailed flow features and affect the corresponding gas transport in the lung. Since it is not clear if the Marangoni effect could encourage (discourage) the convection to improve (impede) the gas transport, it is essential to study the thick-layer alveolar flow, particularly in the presence of surfactant prior to analyzing the corresponding gas transport.

Previous studies have examined airflow in alveoli without an air-liquid interface.[7,8] It would be interesting to examine the effect of such an interface on the flow fields determined in those works. In these studies, the alveolus remains a self-similar shape during breathing, and the associated fluid motions are governed by quasisteady Stokes flows. The resulting flow field exhibits self-similar patterns with a zero cycle-average due to reversibility of Stokes flow. For the transport of large particles such as aerosols, such flow fields result in chaotic mixing as demonstrated by particle trajectories.[8] In this regard, we are also interested in how the presence of the liquid layer modifies the mixing features for the transport of large particles, particularly in the presence of surfactant. This again requires the flow analysis prior to further addressing the above question.

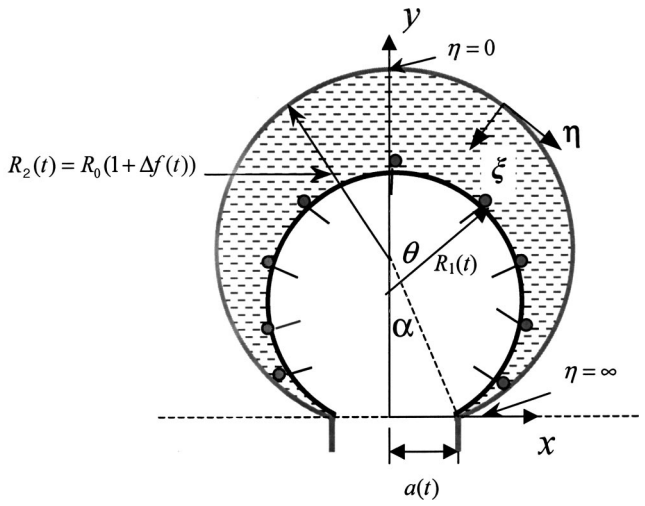

FIG. 2. The geometry for modeling thick-layer alveolar flows. The motion of the alveolar wall is self-similar such that the opening angle α remains fixed during breathing.

The present paper investigates the flow and surfactant transport in a thick fluid layer in an alveolus with prescribed breathing motions. The paper is organized as follows. We present the model formulation in Sec. II. In Sec. III we combine analytical and numerical techniques to solve for the flow field and surfactant concentration. The results and discussion are presented in Sec. IV. We also compare with previous studies and discuss physiological applications in Sec. V. Conclusion is in Sec. VI.

II. MATHEMATICAL MODEL

Consider a thick fluid layer coating the interior of a single alveolus shown in Fig. 2. The model system is two dimensional. The alveolus is assumed to be a circular cap with an opening width $a^*(t^*)=a_0[1+\Delta f(t^*)]$, where a_0 is the mean opening width, $a_0\,\Delta$ is the breathing amplitude, and $f(t^*)$ is a time-dependent function prescribed for breathing. Following the alveolar model of Haber *et al.*,[8] the motion of the alveolar wall during breathing is self-similar, so the alveolar opening angle remains constant during breathing. We further assume that the fluid is pinned at the alveolar opening and the volume of the fluid during breathing is thus conserved. This pinned condition for the fluid motions is a reasonable approximation for an alveolus with sufficient liquid volume since the flow rate across the liquid layer at the proximity of the alveolar rim is expected to be negligible.

For nondimensionalizing the flow system, let a_0, ω^{-1}, ωa_0, and $\mu\omega$ be length, time, velocity and pressure scales, respectively. Also let σ_0^* be the surface tension at the reference state and the corresponding surfactant concentration be Γ_0^*. Since $a_0 \sim 100\ \mu$m, both Reynolds number $\mathrm{Re}=\rho\omega a_0^2/\mu$ (ρ is the fluid density) and Bond number $\mathrm{Bo}=\rho g a_0^2/a_0^*$ (g is the gravitational acceleration) are small, fluid inertia and gravitional effects are negligible. For sufficiently strong surface tension and small surfactant activity, the interface shape remains circular, as we shall justify later. As such, it is convenient to use two-dimensional bipolar coordinates to describe the flow system. Let (ξ,η) denote two directions in the bipolar coordinates shown in Fig. 2. The geometrical relation between (ξ,η) and Cartesian coordinates (x,y) is also depicted. Then positions of the liquid-gas interface and alveolar wall are given by $\xi=\xi_1(t)$ and $\xi=\xi_2(\xi_1>\xi_2)$, respectively. It can be shown that ξ_2 is equal to half of the opening angle 2α and remains fixed during self-similar breathing.[8] Let the (dimensionless) velocity vector be $\mathbf{v}=(u,v)$, where velocity components (u,v) correspond to (ξ,η) directions, and the pressure be p. Therefore, the governing equations are the continuity equation and the quasisteady Stokes flow equation:

$$\boldsymbol{\nabla}\cdot\mathbf{v}=0, \tag{1}$$

$$\nabla^2\mathbf{v}=\boldsymbol{\nabla}p. \tag{2}$$

Similar to Haber *et al.*,[8] the boundary condition at the moving wall boundary is given by

$$\mathbf{v}=\dot{R}_2[(1+\cos\theta_2\cos\xi_2)\mathbf{i}_r-\sin\theta_2\cos\xi_2\mathbf{i}_{\theta_2}]_{r=R_2}. \tag{3}$$

$R_2(t)$ is the time-dependent radius of the circular wall. Dot denotes the time derivative. The origin of the polar coordinate system (r,θ_2) is located at the center of the circular wall surface. θ_2 is measured in the clockwise sense from the y axis. Evaluating the velocity at the alveolar opening ($\theta_2=\pi-\xi_2$) using (3) is

$$\mathbf{v}[x=a(t),y=0]=\dot{a}\mathbf{i}_x. \tag{4}$$

It is convenient to assume the moving line containing the alveolar entrance to have a velocity

$$\mathbf{v}(x,y=0)=\frac{\dot{a}}{a}x\mathbf{i}_x. \tag{5}$$

This velocity is purely horizontal and varies linearly with respect to the distance to the plane of symmetry so as to maintain a uniform strain in the alveolar tissue. Notice that (4) is also a consequence of (5).

At the air-liquid interface, the no-penetration condition yields

$$\mathbf{v}\cdot\mathbf{n}=\dot{R}_1\mathbf{i}_r \text{ at } r=R_1(t), \tag{6}$$

where $\mathbf{n}$ is the unit normal to the interface (pointing outward) and $R_1(t)$ is the radius of curvature of the interface. $R_1(t)$ or $\xi_1(t)$ can be determined by the conservation of the fluid volume, i.e., flow rates across the wall and the interface are equal. The normal stress condition along the interface is given by

$$-p+\mathbf{n}\cdot[\boldsymbol{\nabla}\mathbf{v}+(\boldsymbol{\nabla}\mathbf{v})^T]\cdot\mathbf{n}=\frac{1}{\mathrm{Ca}}\sigma(\Gamma)\nabla_s\cdot\mathbf{n} \text{ at } r=R_1(t). \tag{7}$$

The capillary number is $\mathrm{Ca}=\mu\omega a_0/\sigma_0^*$. the surface tension σ is a function of the surface concentration Γ and a linear equation of state is applied:

$$\sigma=1-E(\Gamma-1). \tag{8}$$

The surfactant activity is measured by the elasticity number $E=-\Gamma_0^*(\partial\sigma^*/\partial\Gamma^*)_{\Gamma_0^*}/\sigma_0^*$. For a small E and moderate varia-

tion of Γ, the variation of σ is expected to be small and the linear form (8) may be proper. In addition, since Ca is small in the alveolus (10^{-5}), the interfacial curvature dominates in (7) and is spontaneously constant along the interface. Balancing the pressure in (7) gives $p \sim O(\mathrm{Ca}^{-1})$. Thus the pressure dominates the viscous term in (2) and the equation of motion is quasistatic. Consequently, the interface is governed by the Young–Laplace equation and has a circular equilibrium shape.

The tangential stress condition along the interface is

$$\mathbf{n} \cdot [\nabla \mathbf{v} + (\nabla \mathbf{v})^T] \cdot \mathbf{t} = \mathrm{Ma} \nabla_s \Gamma \cdot \mathbf{t} \text{ at } r = R_1(t), \tag{9}$$

where $\mathbf{t}$ is the unit tangent along the interface and the Marangoni number is $\mathrm{Ma} = E/\mathrm{Ca}$. The right-hand side of (9) is the Marangoni stress.

Finally, the surfactant distribution is governed by the conservation equation[9]

$$\Gamma_t - \dot{\mathbf{X}} \cdot \nabla_s \Gamma + \nabla_s \cdot (\mathbf{v}_s \Gamma) + u_n (\nabla_s \cdot \mathbf{n}) \Gamma - \frac{1}{\mathrm{Pe}_s} \nabla_s^2 \Gamma = j, \tag{10}$$

where $\mathbf{X}$ is the interface position in the Cartesian coordinate system (Fig. 2). $\mathbf{v}_s$ is the tangential fluid velocity, u_n is the normal component of the surface velocity, $\mathrm{Pe}_s = \omega a_0^2 / D_s$ is the surface Péclet number (D_s is the surface diffusivity), and j is the sorptive flux which is zero for insoluble surfactant. Note that as pointed out by Wong, Rumschitzki, and Maldarelli,[9] combining the first and second terms of (10) represents taking the time derivative along the direction normal to the surface.

We define s to be the arc-length variable along the interface measured from the line of symmetry. Then the boundary condition for (10) at the symmetry line is $\partial \Gamma / \partial s = 0$. The boundary condition at the alveolar opening could depend on types of an alveolus of interest. For the type A alveolus, we assume no surfactant or liquid transport between adjacent alveoli. Therefore the total amount of surfactant in the alveolus must be conserved. We show in Sec. III that the boundary condition $\partial \Gamma / \partial s = 0$ at the alveolar opening satisfies this requirement. For the type B alveolus that is directly connected to an airway, a thin liquid layer along an airway could carry surfactant in or out of the alveolus. In this case we fix the surfactant concentration at the alveolar opening and set $\Gamma = 1$. It also worth pointing out that applying the pinned condition for the interface (i.e., conserving the liquid volume) for solving the flow field is a good approximation since, for an alveolus with sufficient liquid volume, the flow rate across the thin liquid layer in the proximity of the alveolar opening is expected to be negligible. In this paper, we should apply both types of the boundary conditions for Γ at the alveolar opening to examine how they affect the features of flow and transport.

III. SOLUTION METHOD

With the general formulation above, we seek the solution of the system in the bipolar coordinates (ξ, η). A description of this system is given by Happel and Brenner:[10]

$$x = a(t) \frac{\sinh \eta}{\cosh \eta - \cos \xi}, \quad y = a(t) \frac{\sin \xi}{\cosh \eta - \cos \xi}. \tag{11}$$

The wall and the interface locations are given by $\xi = \xi_2$ and $\xi = \xi_1(t)$. The line of symmetry is at $\eta = 0$. The alveolar openings are located at $\eta = \pm \infty$. We then introduce a stream function ψ defined by

$$u = -\frac{(\cosh \eta - \cos \xi)}{a(t)} \frac{\partial \psi}{\partial \eta}, \quad v = \frac{(\cosh \eta - \cos \xi)}{a(t)} \frac{\partial \psi}{\partial \xi}, \tag{12}$$

which satisfies the continuity equation (1). The Stokes equation (2) for ψ reduces to

$$\nabla^2 \nabla^2 \psi = 0, \tag{13}$$

where the Laplacian in the bipolar coordinates is given by

$$\nabla^2 = \frac{(\cosh \eta - \cos \xi)^2}{a(t)^2} \left(\frac{\partial^2}{\partial \xi^2} + \frac{\partial^2}{\partial \eta^2} \right).$$

Rewriting boundary conditions in terms of the bipolar coordinates and the stream function equation (3) for the normal velocities at the wall yields

$$\psi(\xi = \xi_2) = a \dot{R}_2 \sin \xi_2 \{ \tan^{-1} [\cot(\xi_2/2) \tanh(\eta/2)] + F(\xi_2, \eta) \}, \tag{14a}$$

where

$$F(\xi, \eta) = \frac{\sinh \eta}{(\cosh \eta - \cos \xi)} + 2 \cot \xi \tan^{-1} [\cot(\xi/2) \tanh(\eta/2)].$$

Since $\psi(\xi_2, \eta = 0) = 0$, $\psi(\xi_2, \eta \to \infty)$ then should represent half the flow rate across the wall:

$$\psi(\xi_2, \eta \to \infty) \to R_2 \dot{R}_2 \left[(\pi - \xi_2) + \tfrac{1}{2} \sin(2\xi_2) \right]. \tag{14b}$$

The tangential velocity on the wall yields

$$\psi_\xi(\xi = \xi_2) = -a \dot{R}_2 \sin \xi_2 \cos \xi_2 \frac{\sinh \eta}{(\cosh \eta - \cos \xi_2)^2}. \tag{15}$$

At the interface, the no-penetration condition (5) yields

$$\psi(\xi = \xi_1) = a(\dot{R}_1 \sec \xi_1 - \dot{a} \tan \xi_1) F(\xi_1, \eta) + 2a\dot{a} \tan^{-1} [\cot(\xi_1/2) \tanh(\eta/2)]. \tag{16a}$$

The quantity

$$\psi(\xi_1, \eta \to \infty) \to a(\dot{R}_1 \sec \xi_1 - \dot{a} \tan \xi_1) + R_1 \dot{R}_1 (\pi - \xi_1) \tag{16b}$$

represents half the flow rate across the interface. The right-hand sides of (14b) and (16b) are equal since the liquid volume is conserved. The tangential stress condition at the interface, (9), becomes

$$\frac{\partial u}{\partial \eta}+\frac{\partial v}{\partial \xi}+\frac{1}{(\cosh\,\eta-\cos\,\xi)}(u\,\sinh\,\eta+v\,\sin\,\xi)=-\,\mathrm{Ma}\frac{\partial \Gamma}{\partial \eta}, \tag{17}$$

where u and v are defined in terms of ψ in (12).

We follow the approach similar to Haber *et al.*[8] to construct the solution of the Stokes flow. In order to obtain a convergent numerical solution, ψ is decomposed into two parts,

$$\psi=\psi_1+\psi_2. \tag{18}$$

ψ_1 represents the flow contribution without the alveolar wall while ψ_2 is the disturbance flow field caused by the alveolar boundary. ψ_1 is chosen based on the flow mechanism. The wall motion induces a flow entering or leaving out of the alveolus. Alternatively, the wall motion can be regarded as a response to an external imposed flow such that the total flow rate across the wall is the same as that of the external source in order to conserve the liquid volume. When the wall boundary is absent, the flow field is equivalent to flow through a time-varying slit, i.e., two-dimensional (2D) Sampson flow.[11] This suggests that the Sampson flow should be included in ψ_1. In addition, the speed of the opening linearly varies in x as indicated by (5) and the motion of the opening does not induce a flow rate across the alveolar entrance. These effects can be incorporated into ψ_1 by using an ideal stagnation flow. Thus

$$\psi_1=Q\left[1-\frac{2}{\pi}[\sin^{-1}Z-Z(1-Z^2)^{1/2}]\right]-a\dot{a}xy, \tag{19}$$

where

$$Z=\frac{1}{a(t)\sqrt{2}}[a^2-x^2-y^2+\sqrt{(x^2+y^2-a^2)^2+4a^2y^2}]^{1/2}.$$

For (19) the first and the second terms are the 2D Sampson flow[11,12] and an ideal stagnation flow, respectively. (19) can be written in terms of ξ and η using (11) to substitute for x and y. The disturbance part ψ_2 can be written as an infinite series,

$$\psi_2=\frac{1}{(\cosh\,\eta-\cos\,\xi)}\sum_{n=1}^{\infty}\hat{\phi}_n(\xi)\sin(k_n\eta), \tag{20a}$$

$$\begin{aligned}\hat{\phi}_n=&A_n\left[\frac{\cos(\xi-\xi_2)\sinh[k_n(\xi-\xi_2)]}{\cos(\xi_1-\xi_2)\sinh[k_n(\xi_1-\xi_2)]}-\frac{\sin(\xi-\xi_2)\cosh[k_n(\xi-\xi_2)]}{\sin(\xi_1-\xi_2)\cosh[k_n(\xi_1-\xi_2)]}\right]\\&+B_n\left[\frac{\cos(\xi_1-\xi)\sinh[k_n(\xi_1-\xi)]}{\cos(\xi_1-\xi_2)\sinh[k_n(\xi_1-\xi_2)]}-\frac{\sin(\xi_1-\xi)\cosh[k_n(\xi_1-\xi)]}{\sin(\xi_1-\xi_2)\cosh[k_n(\xi_1-\xi_2)]}\right]\\&+C_n\left[\cos(\xi-\xi_1)\frac{\sinh[k_n(\xi-\xi_2)]}{\sinh[k_n(\xi_1-\xi_2)]}\right]\\&+D_n\left[\cos(\xi_2-\xi)\frac{\sinh[k_n(\xi_1-\xi)]}{\sinh[k_n(\xi_1-\xi_2)]}\right],\end{aligned} \tag{20b}$$

where $k_n=n\pi/\eta_m$ and η_m corresponds to the location of the alveolar opening. While the exact location of the alveolar opening is at $\eta_m\to\infty$, in practice, $\eta\sim 5$ has already reached the location of at most 0.5% (based on the opening width $2a$) away from the edge of the alveolar rim, i.e., $y\sim 0.01a$ or less. The chosen value $\eta_m=10$ is sufficiently large to ensure desired numerical accuracy. The time-dependent coefficients A_n, B_n, C_n, and D_n are determined by boundary conditions (14)–(17) with a given surfactant concentration distribution. The system is coupled to the surfactant transport equation, (10), through the tangential stress condition, (17).

The form of (10) in the polar coordinates with respect to the center of the circular interface is much simpler than in the bipolar coordinates. For an insoluble surfactant, (10) in the polar coordinates is

$$\frac{\partial \Gamma}{\partial t}+\frac{\dot{H}_1\sin\,\theta}{R_1}\frac{\partial \Gamma}{\partial \theta}+\frac{1}{R_1}\frac{\partial}{\partial \theta}(u_s\Gamma)+\frac{\Gamma}{R_1}(\dot{R}_1+\dot{H}_1\cos\,\theta)-\frac{1}{\mathrm{Pe}_sR_1^2}\frac{\partial^2\Gamma}{\partial \theta^2}=0, \tag{21}$$

where θ is an azimuthal angle along the interface, and is measured from $\theta=0$ at the symmetry line to $\theta=\pi-\xi_1(t)$ at the alveolar opening. Since the θ domain is time dependent, it is more convenient to introduce a variable $s=\theta/(\pi-\xi_1)$ $(0\leqslant s\leqslant 1)$to have a fixed computational domain. This transforms (21) to become

$$\frac{\partial \Gamma}{\partial t}+\frac{\partial}{\partial s}(f\Gamma)+\Gamma\left(\frac{\dot{R}_1}{R_1}-\frac{\dot{\xi}_1}{\pi-\xi_1}\right)-\frac{1}{\mathrm{Pe}_sR_1^2(\pi-\xi_1)^2}\frac{\partial^2\Gamma}{\partial s^2}=0, \tag{22}$$

where

$$f=\frac{u_s}{R_1(\pi-\xi_1)}+\frac{s\dot{\xi}_1}{\pi-\xi_1}+\frac{\dot{H}_1\sin\,\theta(s)}{R_1(\pi-\xi_1)}.$$

Obviously, $f(s=0)=0$ at the symmetry line. At the alveolar opening, it can be shown that the surface velocity $u_s(s=1)$ is

$$u_s(s=1)=-\,\dot{a}\cos\,\xi_1, \tag{23}$$

which is just a projection of the velocity (5) at the alveolar entrance to the interface. With the aid of the geometrical

constraints $R_1 \sin \xi_1 = H_1$ and $R_1 \sin \xi_1 = a$, the first term of f cancels the rest of the terms exactly at the alveolar opening, i.e., $f(s=1)=0$. Therefore, for no surfactant flux boundary condition at the alveolar opening, integrating (22) along the entire interface in conjunction with $f=0$ at $s=0$ and 1 for ensuring the conservation of the surfactant mass requires no diffusive flux at the moving alveolar opening, i.e., $\partial\Gamma/\partial s = 0$ at $s=1$.

As such, (22) is subject to the following boundary conditions for Γ. At the symmetry line $s=0$,

$$\frac{\partial \Gamma}{\partial s}(s=0)=0. \tag{24}$$

At the alveolar openings $s=1$, the boundary condition is

$$\frac{\partial \Gamma}{\partial s}(s=1)=0 \text{ for type A alveolus,} \tag{25a}$$

$$\Gamma(s=1)=1 \text{ for type B alveolus.} \tag{25b}$$

The numerical procedures for solving the flow field and the surfactant concentration distribution are as follows. For a given surfactant concentration distribution Γ at a time t, we calculate the surface tension gradient (i.e., Marangoni stress) along the interface. We then calculate the corresponding flow field using the stream function formulation. This flow field is applied to update Γ at $t+\Delta t$ by solving the surfactant transport equation (22) numerically. The implicit Euler method is employed to discretize the time derivative. To discretize the spatial derivatives, we apply finite volume scheme[13] in combination with upwind and central differences used for the first and second spatial derivatives, respectively. The form of (22) and the boundary condition (25a) makes the finite volume scheme more appealing than finite differences because the latter is less reliable to control a possible leakage of surfactant mass due to the spatial discretization.

Starting with a uniform surfactant distribution $\Gamma=1$ computations are performed till a time periodic oscillation is reached. For a typical simulation, the number of the spatial grid points Ns=20 and the time step $\Delta t=0.01$ were used. Solutions converged in 600–2000 times steps (1–3 cycles). Convergence was achieved when doubling Ns and halving Δt yielded relative errors of less than 5%. For the system with (25a), grid sizes and time steps were chosen to satisfy the conservation of the surfactant mass to within 1.5%.

IV. RESULTS AND DISCUSSION

In this paper, we would like to take an initial step to understand qualitative flow and transport features that depend on the liquid volume V, the opening angle ξ_2, the breathing amplitude Δ, the Marangoni number Ma, the surface Péclet number Pe_s, and the ratio of inspiration to expiration periods ($I:E$). We are more interested in a diseased situation where the lung is filled with PFC liquid in a level of 90% of the functional residual capacity 30 ml/kg [functional residual capacity (FRC), the volume at the end of expiration] during PLV. If the lung is ventilated with the tidal volume ranging 2.5–25 ml/kg under normal respiratory rate (12 breaths/min), and delivered pulmonary drugs are surface-active agents with $O(1)$ Ma, $V=0.9$, $\Delta=0.2$, $\xi_2=\pi/2$, Ma=4.0, and $\mathrm{Pe}_s=10.0$ are chosen to represent such a situation. Since the $I:E$ in particular plays a critical role in determining the flow and transport features, various $I:E$ ratios (1:1, 1:2, and 2:1) (Ref. 14) are also chosed in order to demonstrate interesting results and subsequent physiological implications. As discussed in Sec. II, type A and B alveoli have different boundary conditions for the surfactant concentration at the alveolar opening. We shall present the results of each case separately to see the role of surfactant and different parameters in determining the flow and transport in different types of alveoli. We first examine the system with an insoluble surfactant and then extend the analysis to the case with a soluble surfactant.

A. Type "A" alveolus: No surfactant flux at the alveolar opening

1. Unsteady streamlines and surfactant concentration distribution

We first examine flow and surfactant transport in the type A alveolus for which a zero surfactant flux is applied at the alveolar opening. The results that we present here have reached time periodic states. For convenience, we choose $t=0$ (2π) to be the moment at the beginning (end) of inspiration (expiration). Figure 3 shows a series of snapshots of typical unsteady streamlines during the breathing cycle for $I:E=1:1$ in which inspiration (expiration) occurs during $t=0-\pi$ ($\pi-2\pi$).

During inspiration [Figs. 3(a)–3(c)], the alveolus expands. Since both the wall and the interface move, the streamlines cross these boundaries. Also since the liquid volume is conserved, whatever streamlines enter the flow domain through the interface leave through the wall. Notice that, at the end of inspiration $t=\pi$ [Fig. 3(d)], the streamlines show a vortex pattern even though the boundaries are at rest. As the alveolus contracts during expiration [Figs. 3(e)–3(g)], streamline patterns are similar to those during inspiration, but with the opposite flow directions. Again, at the end of expiration $t=2\pi$ [Fig. 3(b)], a vortex appears with its flow direction opposite to that at the end of inspiration. The presence of vortices at end inspiration and end expiration when the boundaries are at rest suggests that flows are driven by Marangoni stresses along the interface due to nonuniform surfactant concentrations at these instants. Figure 4 confirms this by showing the corresponding surfactant concentration distribution at different instants during the breathing cycle. Since the total amount of surfactant is conserved, the surfactant concentration becomes lower (higher) as the alveolus expands (contracts) during inspiration (expiration). At the end of inspiration, the surfactant concentration is higher near the symmetry line. Since boundaries are stationary at this moment, this nonuniform surfactant distribution drives a surface flow from the symmetry line toward the alveolar opening, and thus induces a flow recirculation with a counterclockwise direction shown in Fig. 3(d). At the end of expiration, the interfacial surfactant gradient and the surface flow are in the opposite direction leading to a clockwise vortex [Fig. 3(h)].

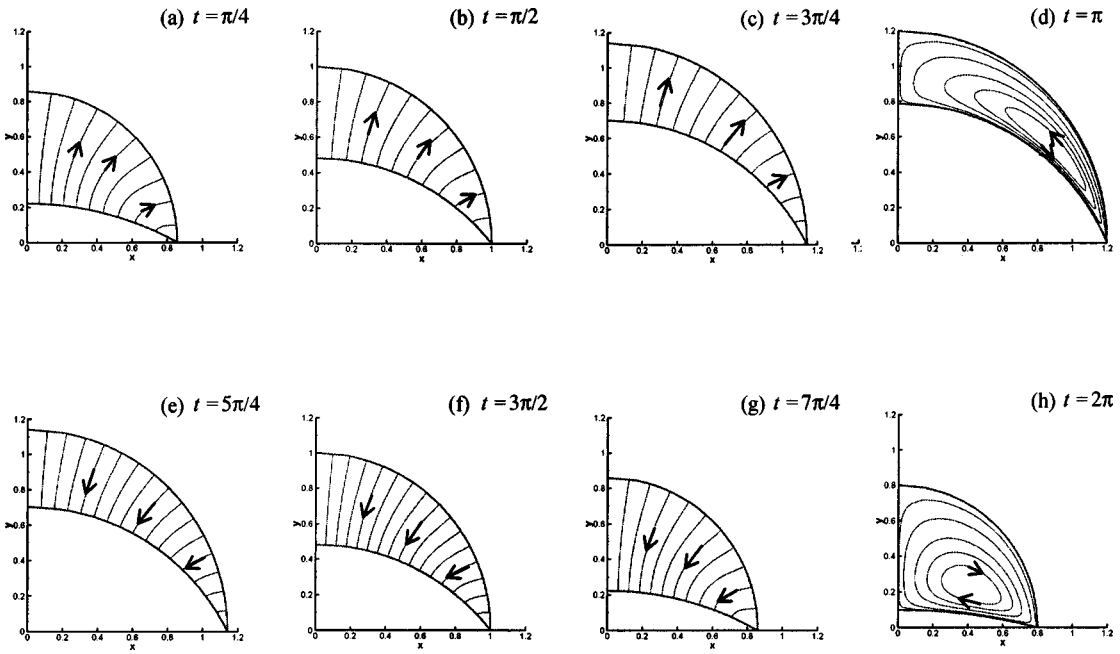

FIG. 3. Snapshots of streamlines during a breathing cycle for the type A alveolus in the presence of an insoluble surfactant. $V=0.9$, $\Delta=0.2$, $\alpha=\pi/2$, Ma $=4$, $\mathrm{Pe}_s=10$, and $I:E=1:1$. The alveolus expands during inspiration [(a)–(d)], while it contracts during expiration [(e)–(h)]. (d) corresponds to the moment of the end of inspiration and (h) is at the end of expiration. Though the alveolus has no motions at the instant of (d) and (h), there are still flows induced by the Marangoni stresses via nonuniform surfactant concentrations along the interface.

2. Cycle-averaged streamlines and surfactant concentration distribution

In the absence of surfactant, there is no cycle-averaged flow for any $I:E$ ratio because the flow system is linear. In the presence of surfactant, a nonlinearity arises from the coupling of the flow field and surfactant concentration in the surface convection terms in (22). The resulting flow contributions during inspiration and expiration are unequal, leading to a nonzero cycle-averaged flow.

We adopt the following procedure to calculate cycle-averaged streamlines. The cycle-averaged wall velocity and normal velocity at the interface are zero. Therefore, the only driving force comes from a nonzero cycle-averaged Marangoni stress along the interface, which is calculated from the cycle-averaged surfactant concentration distribution. The governing equations and boundary conditions for the stream function (13)–(17) are averaged over a cycle. The cycle-averaged stream function can be expressed in terms of an infinite series as in (20) and the coefficients are solved analytically with the previously determined surfactant concentration.

We are particularly interested in the effect of $I:E$ on the cycle-averaged flow and surfactant transport. Figure 5 shows the cycle-averaged steady streamlines for different $I:E$ ratios. For $I:E=1:1$ [Fig. 5(a)], a two-vortex flow structure is seen where the upper vortex has a counterclockwise direction and vortex has a clockwise direction. Thus the surface flow is driven from both the alveolar opening and the symmetry-line end, and moves towards the stagnation point at the middle of the interface. This suggests that the surfactant concentrations at both the alveolar opening and the symmetry line are higher than at other points of the interface, and that the minimum surfactant concentration occurs at the stagnation point along the interface. Figure 5(b) shows the case of $I:E=1:2$ in which the expiration period is longer than inspiration. The resulting cycle-averaged streamlines show a single vortex with clockwise direction. Therefore, the surface flow is driven from the alveolar opening (higher Γ) to the symmetry line (lower Γ). When the $I:E$ ratio is changed to 2:1 the flow still exhibits a single vortex structure [Fig. 5(c)], but its direction is opposite to that of $I:E=1:2$.

Figure 6 shows the corresponding surfactant concentration distributions for different $I:E$ ratios. For $I:E=1:1$, the surfactant concentration only varies slightly along the interface. It has a minimum at $s\sim 0.7$ that corresponds to the stagnation point seen in Fig. 5(a). The Marangoni stress drives the surface flow toward the stagnation point from both ends of the interface, and thus is consistent with the flow pattern of Fig. 5(a). Similarly, the surfactant distributions for $I:E=1:2$ and $I:E=2:1$ support the flow fields seen in Figs. 5(b) and 5(c), respectively. Thus the appearance of vortices is the result of flow being driven from regions of high surfactant concentration to low surfactant concentration.

Figures 5 and 6 suggest that the cycle-averaged flows are rather sensitive to $I:E$ ratios. To understand how $I:E$ plays a role in determining the cycle-averaged flow, it is instructive to examine the surfactant transport equation (22). As inspecting the left-hand side of (22), the effect of the surface convection (the second term) competes that arisen from the surface area expansion/contraction (the third term) during breathing in a following manner. During inspiration, the surface flow tends to sweep surfactants from the alveolar opening toward the symmetry line. On the other hand, the expansion of the surface area tends to diminish surfactant

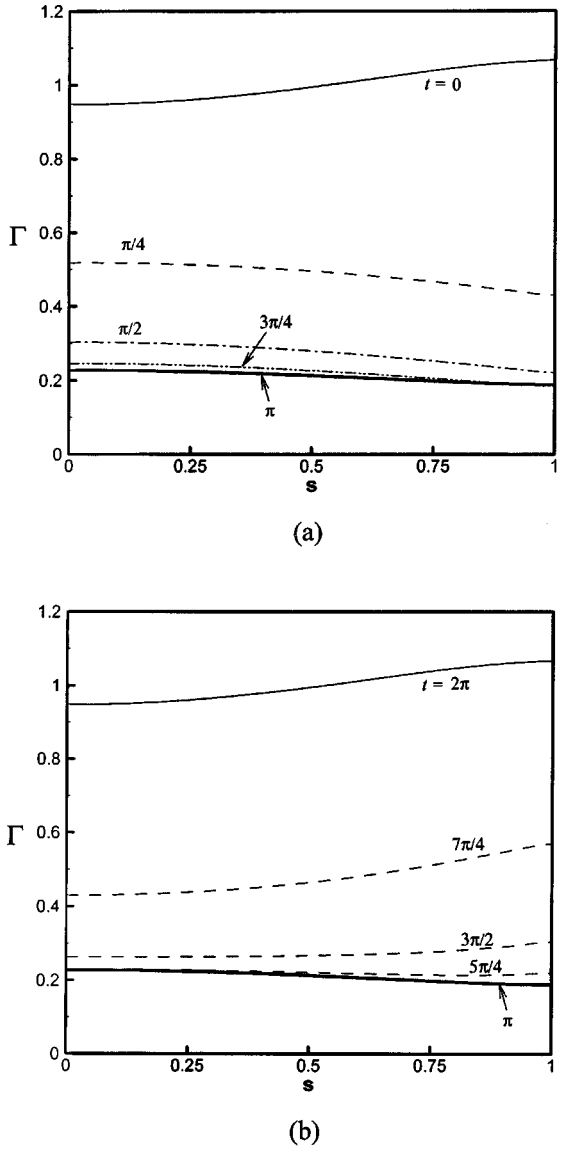

FIG. 4. The surfactant concentration distribution during a breathing cycle for the alveolus A in the presence of an insoluble surfactant. $V=0.9$, $\Delta=0.2$, $\alpha=\pi/2$, Ma=4, $\mathrm{Pe}_s=10$, and $I:E=1:1$. During inspiration as in (a), the alveolus expands and the surfactant concentration level falls as a result of the conservation of the surfactant mass. Similarly during expiration as in (b), the concentration level rises. Notice that though at $t=0$ or π the alveolus has no instant motions, the surfactant concentration distribution is uneven, and thus can induce Marangoni flows as in Fig. 3(d) or 3(h).

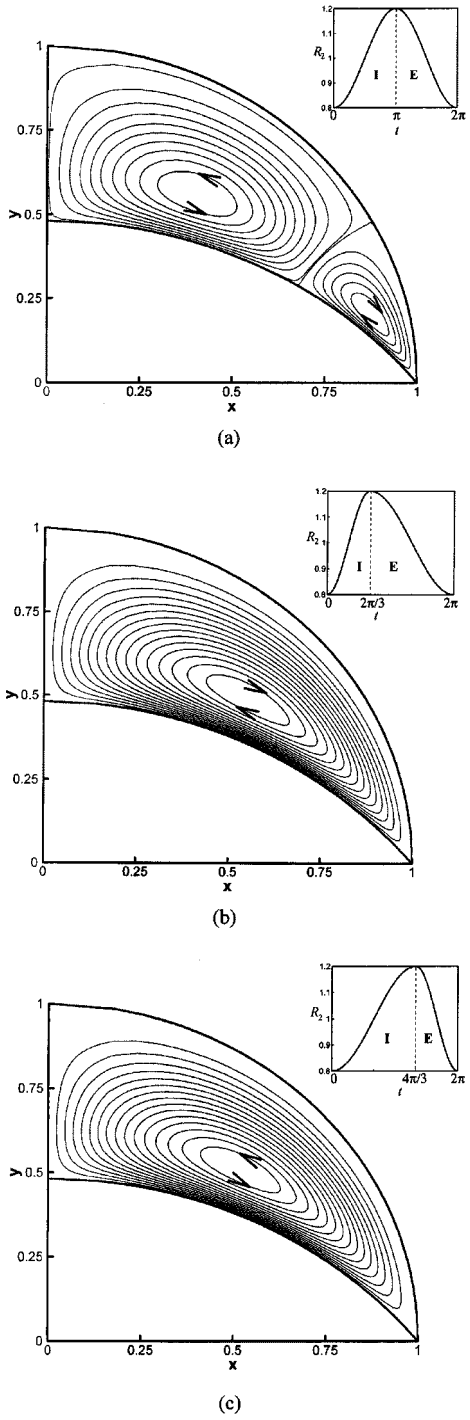

FIG. 5. The cycle-averaged streamlines for the alveolus A in the presence of an insoluble surfactant. The effects of $I:E$ are (a) $I:E=1:1$, (b) $I:E=1:2$, (c) $I:E=2:1$. $V=0.9$, $\Delta=0.2$, $\alpha=\pi/2$, Ma=4, $\mathrm{Pe}_s=10$. For $I:E=1:1$, the streamlines exhibit a two-vortex structure. $I:E=1:2$ has only one vortex with a clockwise flow direction. $I:E=2:1$ also shows a one-vortex pattern, but it has a opposite flow direction to $I:E=1:2$. To explain various flow patterns can be seen in Fig. 6 for the cycle-averaged surfactant concentration distribution.

concentration to a greater extent at the symmetry-line end than that at the alveolar opening. During expiration the trends are reversed.

We note that for $I:E=1:1$, the surfactant concentration at the symmetry line is higher than that at the alveolar opening during most of the inspiration period, while the opposite is true during expiration (Fig. 4). The distribution of the surfactant concentration during a cycle is a result of competition between the surface convection and the surface area stretching/contraction. To illustrate such a competition, the local contribution from each effect is identified via integrating the corresponding term of Eq. (22). The local contribution from the surface convection is indicated by $\mathrm{Ic}=-\int_s^{s+\Delta s}\partial/\partial s(f\Gamma)ds=(f\Gamma)_s-(f\Gamma)_{s+\Delta s}$, and the corresponding surface area part is reflected by $\mathrm{Is}=-[\dot{R}_1/R_1-\dot{\xi}_1/(\pi-\xi_1)]\int_s^{s+\Delta s}\Gamma ds$. Note that the minus sign in front of each integral is used for representing the net change of surfactant mass due to the respective effect. The local contribution Ic and Is for $I:E=1:1$ are then depicted in Figs. 7(a) and 7(b)

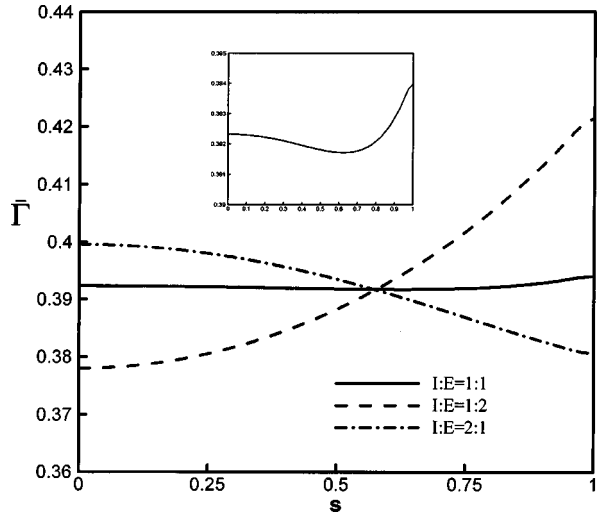

FIG. 6. The effect of $I:E$ on the cycle-averaged surfactant concentration distribution for the alveolus A. $V=0.9$, $\Delta=0.2$, $\alpha=\pi/2$, Ma=4, and $\mathrm{Pe}_s=10$. The zoom-in view is for $I:E=1:1$. Uneven cycle-averaged surfactant concentrations induce Marangoni stresses that drive flow from the higher concentration (lower tension) regions to the lower concentration (higher tension) regions, leading to the vortices seen in Fig. 5.

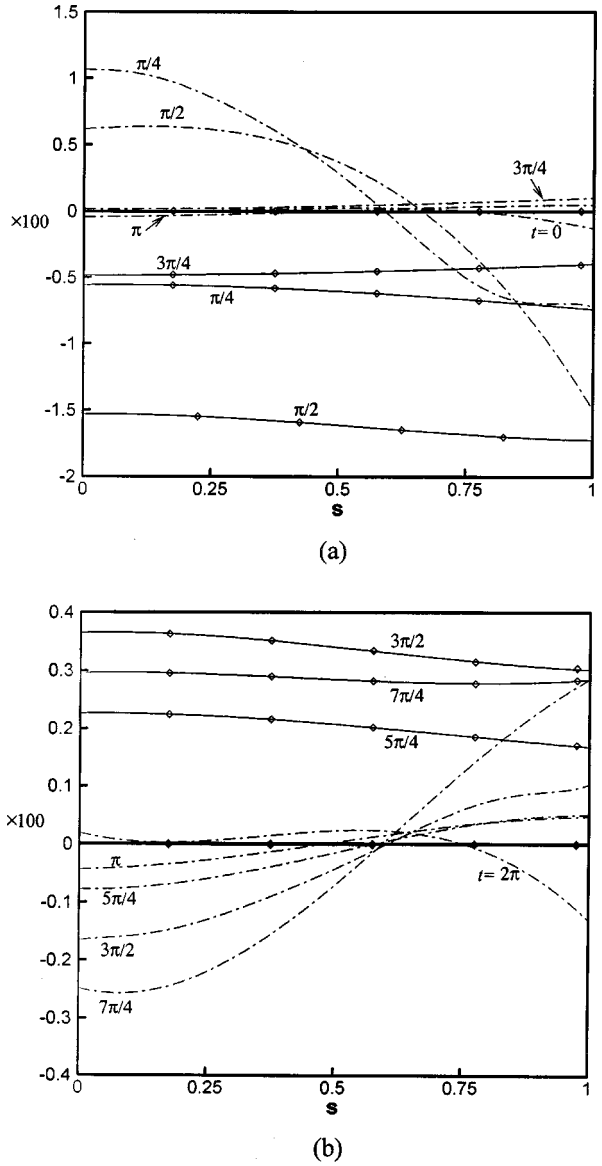

FIG. 7. The local contribution from the surface convection Ic (dash dotted) and the one from the surface area Is (symbol) for the alveolus A in the presence of an insoluble surfactant. $V=0.9$, $\Delta=0.2$, $\alpha=\pi/2$, Ma=4, $\mathrm{Pe}_s=10$, and $I:E=1:1$. (a) Inspiration. (b) Expiration.

for inspiration and expiration, respectively. During inspiration as in Fig. 7(a), $\mathrm{Is}<0$ arises from the dilution due to the surface expansion. Notice that from $t=\pi/4$ to $t=\pi/2$, $\mathrm{Ic}<0$ for $s>0.7$, creating the tendency to lower Γ near the opening end. This tendency persists throughout the rest of inspiration, thus Γ is higher (lower) near the symmetry line (the opening end) during most of inspiration as already revealed in Fig. 4(a). During expiration as in Fig. 7(b), $\mathrm{Is}>0$ due to surface contraction. Since $\mathrm{Ic}>0$ for $s>0.7$ during most of expiration, the resulting surfactant distribution shows higher (lower) Γ near the opening end (the symmetry line). This also can be seen in Fig. 4(b). All above suggest that the surface convection plays a more important role than the surface area in determining the surfactant distribution. Since the cycle-averaged flow patterns derive from the cycle-averaged Marangoni effect that arises from the competition between opposing trends of the surfactant distribution during inspiration and expiration, the role of $I:E$ in determining the cycle-averaged flow patterns now becomes evident. Since longer inspiration (expiration) tends to yield lower (higher) surfactant concentration at the alveolar opening, promoting Marangoni flow towards the alveolar opening (the symmetry line), the cycle-averaged flow for $I:E=2:1$ (1:2) has a counterclockwise (clockwise) vortex structure.

B. Type "B" alveolus: Fixed surfactant concentration at the alveolar opening

The unsteady stream patterns here are similar to those in the no flux case during most of the breathing cycle. However, at end inspiration and end expiration, the flow fields behave differently, as seen in Figs. 8(a) and 8(b) for $I:E=1:1$. A single vortex is seen in each case with clockwise (end inspiration) and counterclockwise (end expiration) directions. These directions are opposite to those in Figs. 3(d) and 3(h) of the no flux case and indicate that the surfactant concentration is higher at the alveolar opening at end inspiration and at the symmetry line at end expiration and varies monotonically in space.

As mentioned earlier in Sec. IV A, surfactant transport mechanisms involve competition between the surface flow and surface area stretching. To understand how the interplay of these mechanisms gives rise to the observed flow patterns, we again examine the surfactant concentration profiles during the cycle, plotted in Fig. 9. At the start of inspiration, the surfactant concentration at the symmetry line is greater than the fixed concentration at the alveolar-opening end, but becomes lower at end inspiration. It then increases during expiration and becomes greater than the alveolar-opening end concentration at end expiration. This explains the flow patterns seen in Fig. 8. To further elucidate the above via identifying how the surface convection and the surface area compete during inspiration and expiration, we again plot the

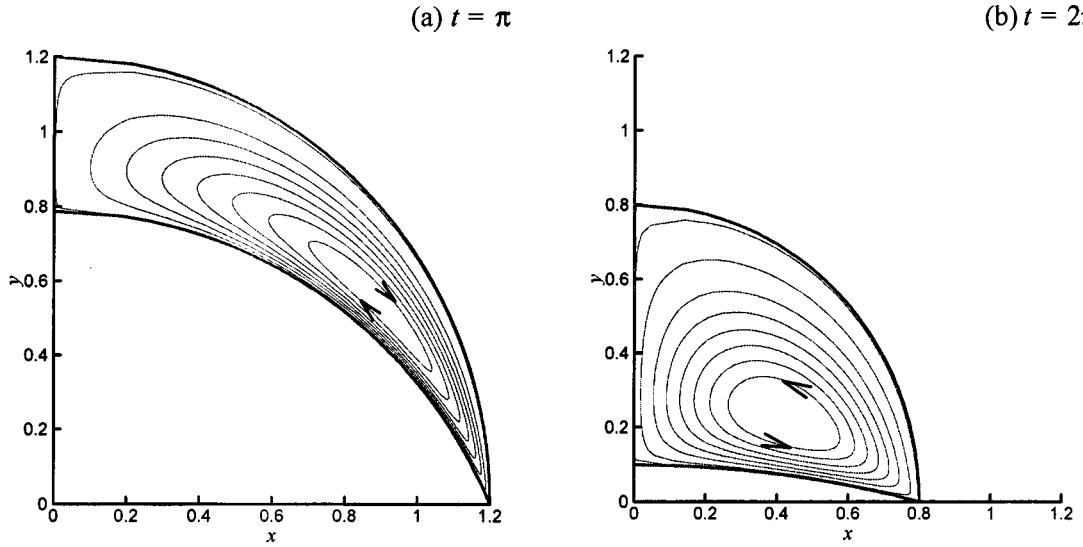

FIG. 8. The streamlines of the alveolus B in the presence of an insoluble surfactant. $V=0.9$, $\Delta=0.2$, $\alpha=\pi/2$, Ma=4, $\mathrm{Pe}_s=10$, and $I:E=1:1$. (a) and (b) are at the end of inspiration and expiration, respectively. The flow directions are opposite to those in the alveolus A at the same instants [Figs. 3(d) and 3(h)].

local contribution from the surface convection Ic and the surface area Is in Figs. 10(a) and 10(b). As in Fig. 10(a) for inspiration, $\mathrm{Is}<0$ is again expected. For $t<\pi/4$, $\mathrm{Ic}<0$ for $s>0.5$, leading to higher Γ near the symmetry line as shown in Fig. 9(a). However, for $t\geqslant\pi/4$, Ic generally >0 for $s>0.4$, resulting in lower Γ near the symmetry line as depicted in Fig. 9(b). These explain Fig. 9(a) and also reveal that the states of lower Γ near the symmetry line seem to be favorable during inspiration. With similar explanations to the process during expiration as in Fig. 9(b), in contrast to the situation during inspiration, expiration is more favorable to create lower Γ near the opening.

With the above observations in mind, we now turn our attention to the cycle-averaged quantities. Figures 11 and 12 show the cycle-averaged streamlines and surfactant concentration distributions, respectively, for different I:E ratios. In contrast to the no flux case, there is only one vortex for I:E=1:1 [Fig. 11(a)] whose direction is opposite to that of the primary vortex in the no flux case. At I:E=1:2 and 2:1 [Figs. 11(b) and 11(c)], a single vortex is present and their flow directions are opposite to the corresponding no flux cases. Cycle-averaged surfactant concentrations are plotted in Fig. 12 and show that longer inspiration (expiration) leads to lower (higher) surfactant concentration at the symmetry line. In conjunction with the results suggested by Fig. 9 and 10 that the symmetry-line end tends to favor lower surfactant concentration during inspiration (expiration), longer inspiration (expiration) thus promotes the tendency to create lower (higher) surfactant concentration at the symmetry line. This thus explains how I:E affects the cycle-averaged surfactant concentration and the resulting streamlines.

C. Extension to bulk soluble surfactants

The discussion so far has been based on insoluble surfactants. Here we extend our analysis to the case with soluble surfactants. In this case, for simplicity, the dimensional sorption flux j^* is

$$j^* = k_a C_s^* - k_d \Gamma^* = -D(\mathbf{n}^* \cdot \boldsymbol{\nabla}^* C^*)_s, \tag{26}$$

where k_a and k_d are adsorption and desorption parameters, respectively, and D is the molecular diffusivity. Note that C_s^* is the sublayer bulk concentration underneath the interface. We choose the concentration scales as the bulk concentration $C_0^*=\Gamma_0^* k_d/k_a$, which is in equilibrium with Γ_0^*. The dimensionless form of (26) can be written as

$$j = K(C_s - \Gamma) = -\frac{1}{\beta \mathrm{Pe}}(\mathbf{n} \cdot \boldsymbol{\nabla} C)_s, \tag{27}$$

where $K=k_d/\omega$ is the sorption parameter, $\beta=k_a/(a_0 k_d)$ is the solubility, and $\mathrm{Pe}=\omega a_0^2/D$ is the bulk Péclet number. The dimensionless governing equation for the bulk surfactant concentration is

$$\frac{\partial C}{\partial t} + \mathbf{v} \cdot \boldsymbol{\nabla} C = \frac{1}{\mathrm{Pe}} \nabla^2 C. \tag{28}$$

The boundary condition along the symmetry line requires

$$\frac{\partial C}{\partial \eta}(\eta = 0) = 0. \tag{29}$$

We assume that there is no surfactant flux across the alveolar wall, namely,

$$\frac{\partial C}{\partial \xi}(\xi = \xi_2) = 0. \tag{30}$$

At the alveolar opening, similar to the boundary conditions for Γ, the boundary condition for C could be either

$$\frac{\partial C}{\partial \eta}(\eta \to \infty) = 0 \tag{31a}$$

or

$$C(\eta \to \infty) = 1. \tag{31b}$$

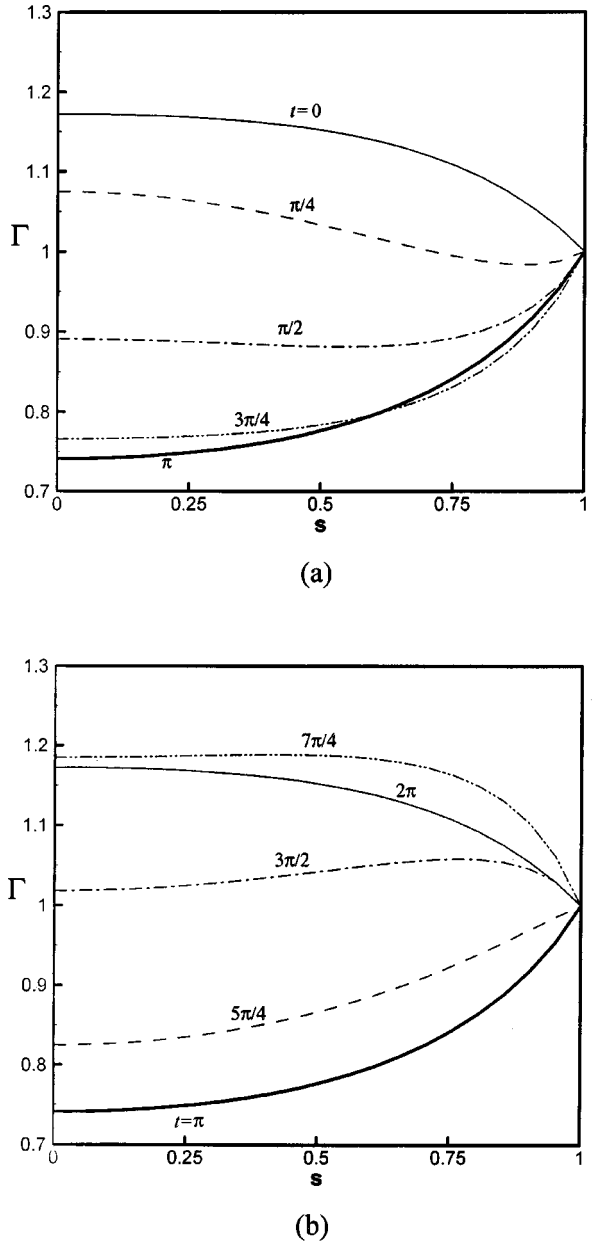

FIG. 9. The surfactant concentration distribution during a breathing cycle for the alveolus B in the presence of an insoluble surfactant. $V=0.9$, $\Delta=0.2$, $\alpha=\pi/2$, Ma$=4$, Pe$_s=10$, and $I:E=1:1$. (a) Inspiration. (b) Expiration.

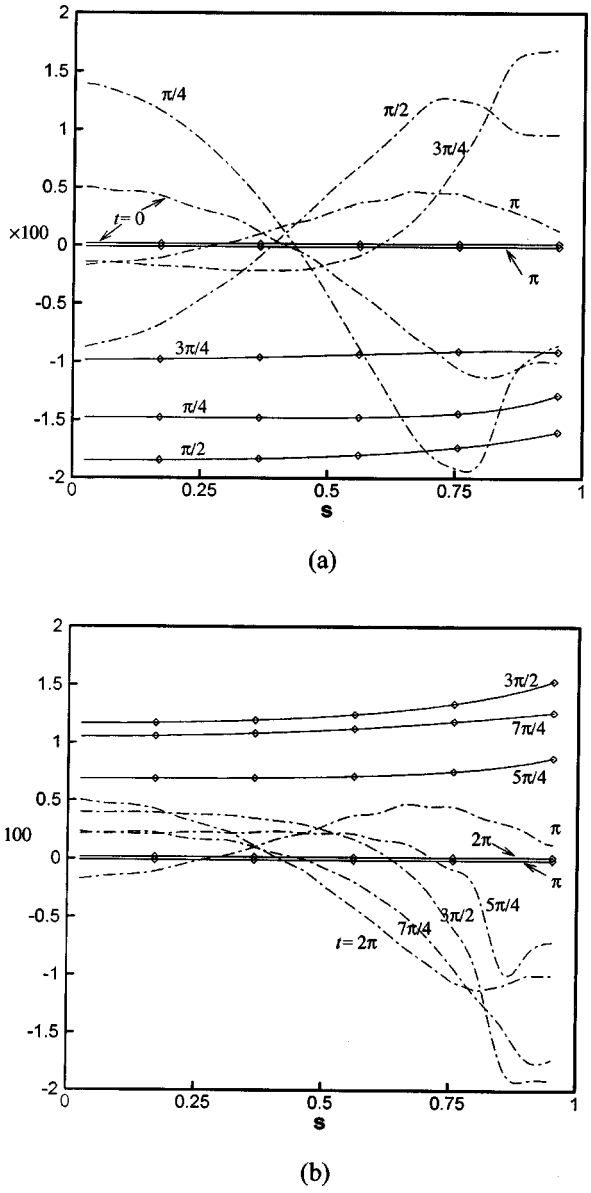

FIG. 10. The local contribution from the surface convection Ic (dash dotted) and the one from the surface area Is (symbol) for the alveolus B in the presence of an insoluble surfactant. $V=0.9$, $\Delta=0.2$, $\alpha=\pi/2$, Ma$=4$, Pe$_s=10$, and $I:E=1:1$. (a) Inspiration. (b) Expiration.

The boundary conditions (31a) and (31b) for C correspond to (25a) and (25b) for Γ, respectively. It is difficult to solve the general problem with soluble surfactant due to the coupling between the flow field, the surface concentration and the bulk concentration. It requires *spontaneously* solving for the flow field, the interfacial, and the bulk transports of surfactant. This not only needs a more sophisticated numerical scheme, but also implementation becomes more time consuming. To assess the effect of a soluble surfactant without the above difficulties, we consider the case in the limit of fast bulk diffusion. As such, both analyses for insoluble surfactant and soluble surfactant with fast bulk diffusion at least could complementarily capture qualitative features prior to performing a more complete analysis. The former can be regarded as a limiting case of slow bulk diffusion (Pe$\to\infty$) while the latter can be viewed as the limit of fast bulk diffusion (Pe$\to 0$). Therefore, the effect of bulk diffusion on the qualitative flow and transport features should lie between these two limiting cases.

If the bulk diffusion at the interface is sufficiently fast such that $(\beta\mathrm{Pe})^{-1}$ is large enough, then the diffusive flux $\mathbf{n}\cdot\nabla C$ in (28) is $O(\beta\mathrm{Pe})\ll 1$. This indicates that, at the leading order in βPe, there is no surfactant flux at the interface. Below, we again examine two situations corresponding to the boundary conditions (31a) and (31b), respectively.

1. Type "A" alveolus: No surfactant flux at the alveolar opening

For the system with the boundary conditions (30) and (31a), there is no surfactant flux across the boundaries anywhere at the leading order in βPe. This suggests that, if the

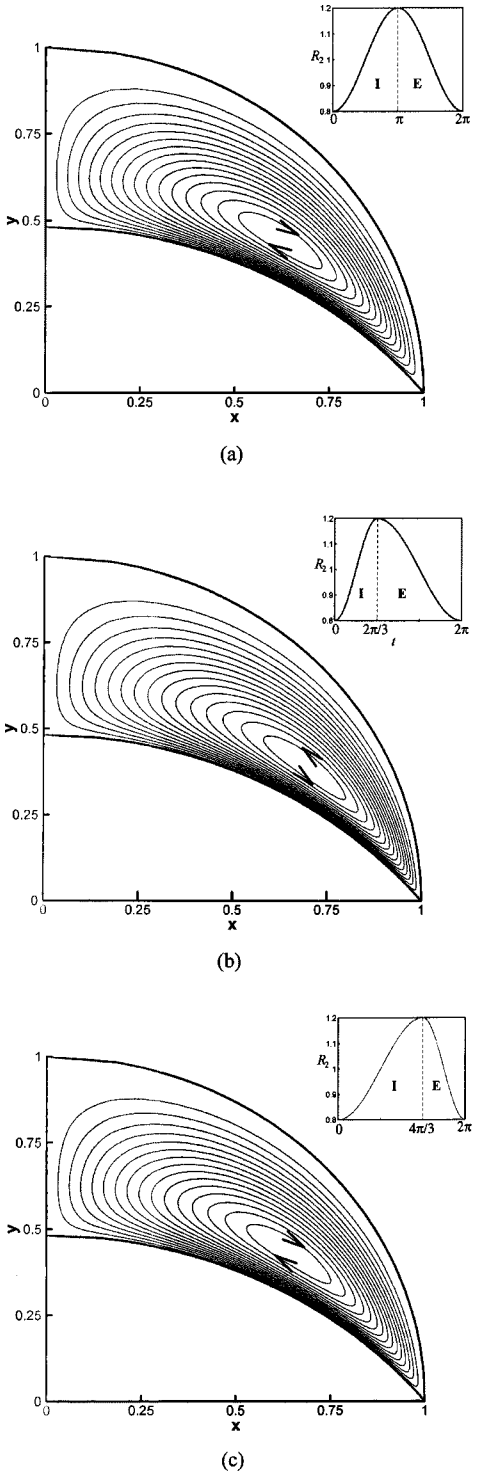

FIG. 11. The cycle-averaged streamlines for the alveolus B in the presence of an insoluble surfactant. The effect of $I:E$: (a) $I:E=1:1$, (b) $I:E=1:2$, (c) $I:E=2:1$. $V=0.9$, $\Delta=0.2$, $\alpha=\pi/2$, Ma=4, and $\mathrm{Pe}_s=10$. All flow patterns exhibit one-vortex structures. To explain various flow patterns can be seen in Fig. 12 for the corresponding cycle-averaged surfactant concentration distributions.

initial bulk concentration is uniform, then it remains unchanged for all times, i.e., $C=1$ everywhere. Therefore, the sublayer concentration $C_s=1$ and

$$j = K(1-\Gamma). \tag{32}$$

The surfactant transport across the interface is thus dictated by a sorption process. Note that the discrepancy in surfactant

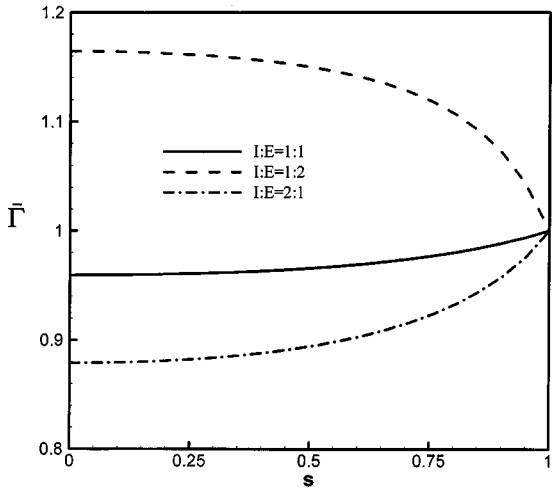

FIG. 12. The effect of $I:E$ on the cycle-averaged surfactant concentration distribution for the alveolus B. $V=0.9$, $\Delta=0.2$, $\alpha=\pi/2$, Ma=4, and $\mathrm{Pe}_s=10$. Uneven cycle-averaged surfactant concentrations induce Marangoni stresses that drive flow from the higher concentration (lower tension) regions to the lower concentration (higher tension) regions, leading to the vortices seen in Fig. 11.

conservation is $O[(\beta\mathrm{Pe})^{-1}]$. The cycle-averaged streamlines with $I:E=1:1$ for different K are shown in Fig. 13. The results for insoluble surfactant [Fig. 5(a)] correspond to $K=0$. Figure 13 shows that an increase in K diminishes the size of the vortex near the alveolar opening, and the flow patterns eventually become one-vortex structures with clockwise flow directions.

The corresponding cycle-averaged surfactant distribution is presented in Fig. 14. As K increases, the surfactant concentration level not only has a smaller deviation from the equilibrium $\Gamma=1$, but also has a less variation so that the local minimum concentration as in the insoluble case no longer appears. This is because a soluble surfactant tends to diminish the surfactant concentration gradients due to constant supply of surfactant from bulk, so does for the Marangoni stress. The resulting surfactant concentration becomes higher as approaching the alveolar opening, and thus induces one-vortex cycle-averaged streamlines.

2. Type "B" alveolus: Fixed surfactant concentration at the alveolar opening

For the system with the boundary condition (31b) there is no flux across the boundaries, except at the alveolar opening, and as a result $C=1$ everywhere. Therefore the sorptive flux is given by (32) in this case also.

Figure 15 shows the cycle-averaged streamlines for $I:E=1:1$ for increasing values of K. Recall that for the insoluble case ($K=0$) there is only one vortex as in Fig. 11(a). However, a soluble surfactant can dramatically modify the flow patterns from one vortex to two or even three vortices, depending on K. When $K=0.5$, a small secondary vortex is seen [Fig. 15(a)]. It is likely that for smaller K the flow still shows one recirculation with clockwise flow direction similar to the insoluble case. More interestingly, for $K=0.7$ [Fig. 15(b)], the flow develops three vortices. When K is increased to 0.8 [Fig. 15(c)], the size of middle recirculation becomes

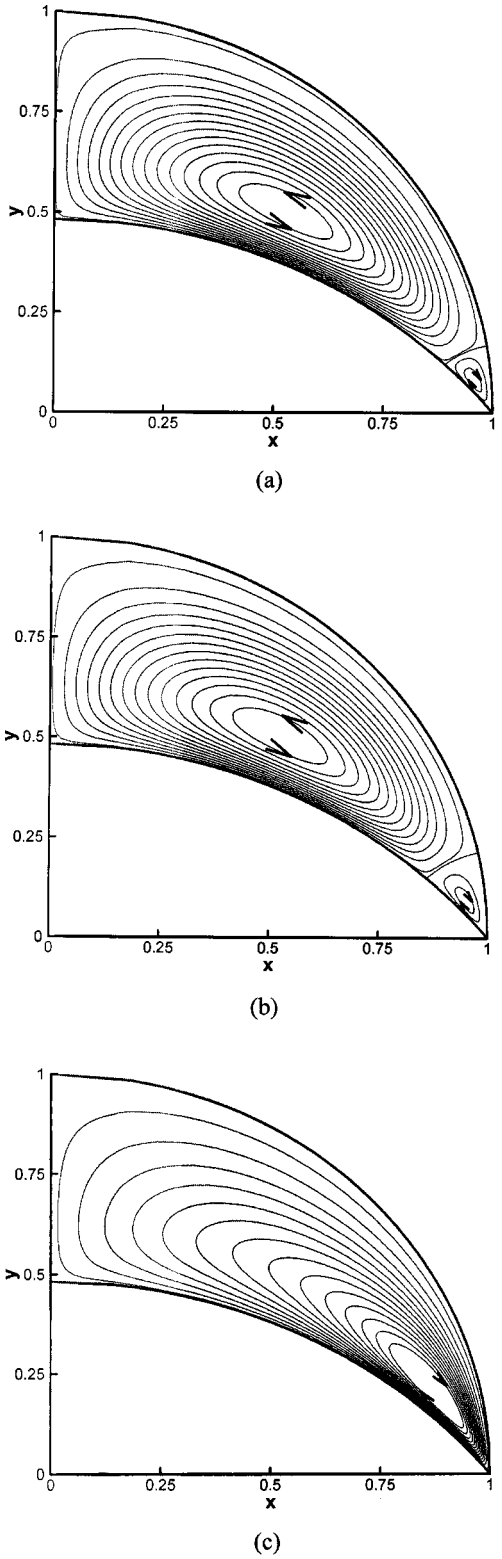

FIG. 13. The cycle-averaged streamlines for the alveolus A in the presence of a soluble surfactant. The effect of sorption parameter K: (a) $K=0.1$, (b) $K=0.2$, (c) $K=0.5$. $V=0.9$, Ma=4.0, $\mathrm{Pe}_s=10$, and $I:E=1:1$.

smaller. At a critical value $K=1$ [Fig. 15(d)], the flow pattern forms a saddle point and an "eye" structure whose two vortices have the same flow direction. At large K the flow again exhibits two vortices [Fig. 15(e)]. These results indicate a transition between three-vortex and two-vortex flow patterns occurs at $K=1$.

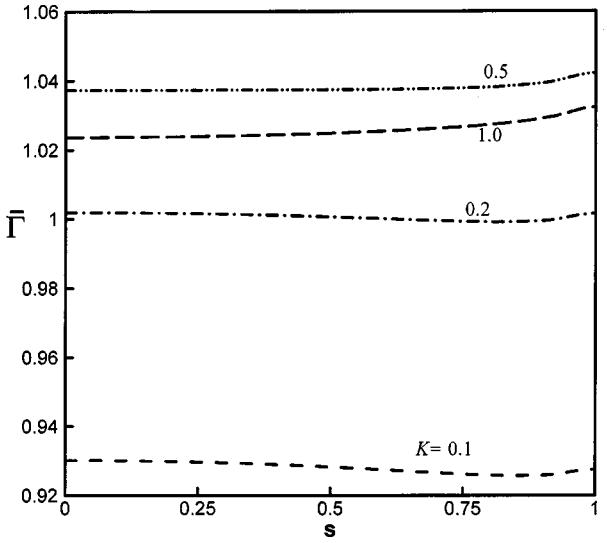

FIG. 14. The effect of K on the cycle-averaged surfactant concentration distribution for the alveolus A in the presence of a soluble surfactant. $V=0.9$, $\Delta=0.2$, $\alpha=\pi/2$, Ma=4, $\mathrm{Pe}_s=10$, and $I:E=1:1$.

The above flow patterns can be explained using the cycle-averaged surfactant concentration distribution in Fig. 16. When $K=0$, the surfactant concentration increases monotonically with increasing s in the vicinity of the alveolar opening. For $K=0.5$, the surfactant concentration shows a maximum near the alveolar opening, which thus induces a two-vortex cycle-averaged flow pattern as in Fig. 15(a). For $K=0.6-0.8$, there is a local minimum and maximum for the surfactant distribution. Such surfactant distributions induce three-vortex cycle-averaged flow streamlines. For $K=1$, the surfactant concentration decreases as approaching the alveolar opening. A saddle point occurs at $s\sim0.75$ where both the first and second derivatives $\partial\Gamma/\partial s$ and $\partial^2\Gamma/\partial s^2$ are zero. Since the surfactant concentration has neither a local maximum nor local minimum along the interface, the resulting surface flow is driven only in the direction toward the alveolar opening. The corresponding flow within the liquid layer tends to be slower as it approaches the saddle point and faster away from it. Thus the flow pattern forms an eye-like, two-vortex structure.

V. COMPARISON WITH PREVIOUS STUDIES AND PHYSIOLOGICAL APPLICATIONS

We compare our results to previous studies of thin liquid films in alveoli to see how alveolar flow and transport behave differently in the two cases. Results for the two types of alveoli with different boundary conditions are compared separately. Wei *et al.*[5] examined thin-layer alveolar flows in type A alveoli and showed that for $I:E=1:1$ and insoluble surfactant, the cycle-averaged flows are directed toward the alveolar opening when the surface tension is sufficiently small. The corresponding cycled-averaged velocity is about 10^{-5} cm/s. However, our thick-layer results for the type A alveolus demonstrates that for $I:E=1:1$ the cycle-averaged flow could exhibit a two-vortex structure having a stagnation

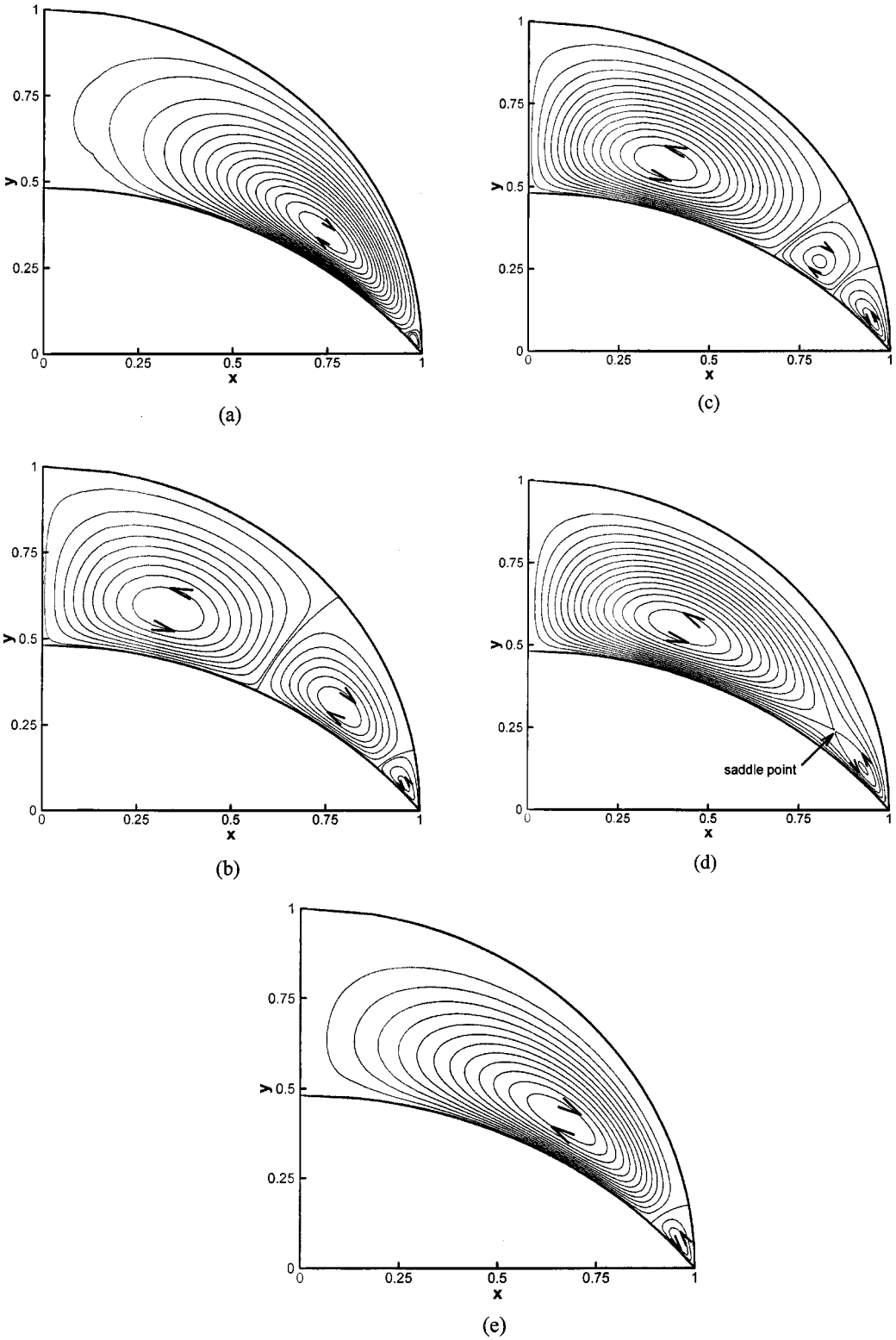

FIG. 15. The time-averaged streamlines for the alveolus B in the presence of a soluble surfactant. The effect of sorption parameter K: (a) $K=0.5$, (b) $K=0.7$, (c) $K=0.8$, (d) $K=1.0$, (e) $K=10$. $V=0.9$, Ma$=4.0$, Pe$_s=10$, and $I:E=1:1$. For an insoluble surfactant ($K=0$) as in Fig. 11(a), there is only one recirculation. As increasing K, the streamlines can appear three recirculations (b) and (c), or even exhibit a saddle-point structure (d).

point on the interface. The surface flow is directed toward the stagnation point from both the alveolar opening and the symmetry line. The estimated cycle-averaged velocity is 10^{-6} cm/s slower than the thin-layer case.

Podgorski and Gradon[15] used a two-dimensional model to examine the flow and transport in a type B alveolus with insoluble surfactant. Their results also suggested that the flow direction is toward the alveolar opening. Similar results were seen in their later three-dimensional, axisymmetric alveolar model.[2] Our thick-layer analysis for the type B alveo-

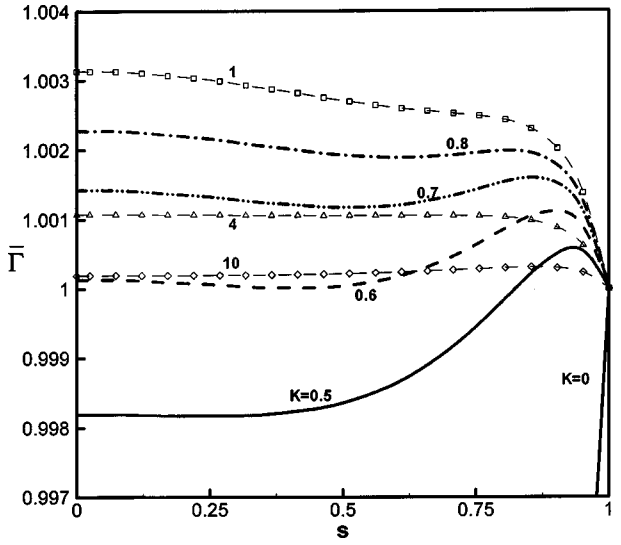

FIG. 16. The effect of K on the cycle-averaged surfactant concentration distribution for the alveolus B in the presence of a soluble surfactant. $V=0.9$, $\Delta=0.2$, $\alpha=\pi/2$, Ma=4, $\mathrm{Pe}_s=10$, and $I:E=1:1$.

lus shows that for $I:E=1:2$, the surface flow has a similar tendency as the thin-layer case while the opposite is true for $I:E=1:1$.

With the above analyses of the flow and transport in an alveolus, it is instructive to apply them in a viewpoint of physiology. However, prior to inferring any further physiological implication from the current analysis, we should notice the following fact. Although the present analysis is based on the fluid-pinned alveolar opening end that does not allow the fluid to enter or leave out of an alveolus (despite of the fact that surfactant molecules can move in or out of an alveolus), in practice, the fluid thickness in the proximity of the alveolar opening is finite but thin. The pinned condition assumed for the fluid motions at the alveolar opening can be regarded as a condition for the *outer* flow to which the *inner* part, the detailed flow solution near the alveolar opening, is required to match. It could be a good approximation when the inflow or outflow contribution to the entire fluid mass is negligible during a cycle if a sufficient amount of liquid is present in an alveolus. This also implies that the qualitative flow features could be insensitive to the detailed flow conditions at the alveolar opening. The study by Wei *et al.*[5] for thin-layer alveolar flows implies that the qualitative flow features could be insensitive to the detailed flow conditions at the alveolar opening. The influence of the alveolar opening on thick-layer alveolar flows could be even less important than that on the thin-layer case. Therefore, although we apply the pinned condition for approximating the flow situation in the proximity of the alveolar opening, the resulting cycle-averaged interfacial flows could provide tendency for particle transport such as particle cleansing or pulmonary drug delivery, in particular when particles or drugs approach to the alveolar rim. As such, the implication from the current study to particle transport should be treated in the "outer" sense. How detailed particle transport occurs at the alveolar opening should be acquired from the inner solution in which a finite fluid thickness must be taken into account.

The system depends on physiological parameters such as the lung volume at end expiration, i.e., FRC, tidal volume V_T, respiratory rate, and $I:E$. For a normal lung, $V_T=500$ ml and FRC=2100 ml, the breathing amplitude $\Delta \sim V_T/6\mathrm{FRC}=0.04$. However, we are more interested in a diseased lung whose FRC could be smaller. In this case, Δ could be as large as 0.2. A typical respiratory rate is 12 breaths/min and gives $\omega \sim 1.26$. The size of an alveolus is about $2a_0=250$ μm. The surface tension of the liquid used for PLV or SRT is about 20–40 dyne/cm. Thus Ca is about $O(10^{-5})$. We use a pulmonary surfactant with $O(1)$ Ma. A typical liquid dose in PLV is close to FRC, we choose the system having liquid filled with 90% of the end-expiration volume of the alveolus ($V=0.9$) to qualitatively describe such situation. With the above parameters, the estimated steady velocity is an order of magnitude between 10^{-6} and 10^{-4} cm/s over the range of $I:E$. For faster steady velocity via properly controlling $I:E$, it could take about 10 min to deliver pulmonary drugs from a terminal bronchiole into an alveolus. A similar amount of time is required to cleanse foreign particles from an alveolus to airways.

For a normal respiratory rate $I:E=1:2$, a typical steady velocity for the type A alveolus is about 10^{-5} cm/s while it is about 10^{-4} cm/s for the type B alveolus. More interestingly, the steady surface flows in the type B alveolus are toward the alveolar opening, but away from it in the type A alveolus. This can have a significant impact on alveolar cleansing[2] and delivery of clinical agents such as aerosol particles to alveoli. The cycle-averaged flow in type A alveoli is more conducive to delivery deep into alveoli while cleansing processes may be more effective in type B alveoli.

The estimated unsteady velocity is about 10^{-3} cm/s. For the transport of respiratory gas such as oxygen and carbon dioxide across the alveolar liquid layer, the corresponding Péclet number is $O(1)$ for a typical diffusivity 10^{-5} cm^2/s of dissolved gas in liquid. Therefore, convection is comparable to diffusion for the gas transport. For cell-cell signaling processes, the route for alveolar cells to communicate back and forth via signaling molecules could be through the extracellular alveolar liquid layer. In this case, the signaling process could be facilitated by transport processes within an alveolus during breathing. For example, surfactant-associated protein-A (SP-A) is a component of pulmonary surfactant and can serve as a signaling molecule for regulating surfactant secretion.[16] SP-A is typically a large molecule and thus has a low diffusivity ($\leqslant 10^{-6}$ cm^2/s). The estimated Péclet number based on the unsteady velocity is $O(10)$ or larger. The convection could dominate cell-cell signaling processes for surfactant secretion in an alveolus.

With the estimated steady velocity 10^{-6}–10^{-4} cm/s, depending on $I:E$ or K, the corresponding steady Péclet number ranges from $10^{-8}/D_m$ to $10^{-6}/D_m$, where D_m is the molecular diffusivity. Therefore, for large molecules such as drugs or genetic material with low diffusivities ($D_m \leqslant 10^{-8}$ cm^2/s) the convective transport dominates.

VI. CONCLUDING REMARKS

Motivated by the growing recognition of the role of alveolar flow on various respiration therapies such as PLV or SRT, we have developed a model of the flow and surfactant transport within an alveolus partially filled with liquid. We combine analytical and numerical techniques to solve for the flow field and surfactant concentration distribution in an alveolus subject to prescribed breathing motions.

We apply our alveolar flow model to study flow and transport in two types of alveoli with different boundary conditions. The type A alveolus is present in an alveolar cluster in which fluid and surfactant exchange is not possible between adjacent alveoli. The type B alveolus is directly connected to an airway from which surfactant and liquid can be delivered into the alveolus. Cycle-averaged streamlines and surfactant concentration profiles are calculated to characterize the transport features. The stream patterns show various vortex structures and are highly sensitive to the $I:E$ ratio. In the presence of an insoluble surfactant, the cycle-averaged flow for the type A alveolus is generally weaker than that for the type B alveolus.

We extend the analysis to soluble surfactants by assuming a sorption-controlled surfactant transport between the interface and the bulk. Though the presence of soluble surfactants reduces the surfactant concentration gradient and results in relatively weak cycle-averaged streaming, the stream patterns could have complicated features. For example, for the type B alveolus, over a certain range of the sorption parameter K, the cycle-averaged stream pattern shows an interesting flow structure transition from two-to three-vortex formation and even exhibits "cat eyes" with a saddle point within the layer.

We have compared the present thick-layer model with previous results for the thin-layer alveolar flows. The thick-layer model could have a different flow tendency compared to the thin-layer model. This suggests that the amount of liquid in an alveolus is an important factor to determine proper $I:E$ in order to achieve the desired molecular delivery or particle cleansing. Our present study may provide guidance to choose a proper amount of liquid or dosage of surfactant instilling into the lung.

Our present model is based on the assumption that the alveolar walls are impermeable. We have neither accounted for intercellular water penetration nor for natural surfactant generated by epithelial cells of the alveolar walls. Such a permeable-wall condition not only modifies the boundary conditions, but also provides an extra source of fluid and surfactant and may qualitatively affect flow and transport features in the system. While a recent theoretical study[4] has considered the effect of a permeable alveolar wall, it was restricted to a thin-layer alveolar flow model. Future work should incorporate permeable alveolar walls to explore their effects on the flow and surfactant transport within an alveolus.

ACKNOWLEDGMENTS

The research was supported by NASA under Grant No. NAG3-2196, and NIH Grants No. HL41126 and No. HL64373.

[1] J. Bastacky, C. Y. C. Lee, J. Goerke, H. Koushafar, D. Yager, L. Kenaga, T. P. Speed, Y. Chien, and J. A. Clements, "Alveolar lining layer is thin and continuous: low-temperature scanning electron microscopy of rat lung," J. Appl. Physiol. **79**, 1615 (1995).
[2] A. Podgorski and L. Gradon, "An improved mathematical model of hydrodynamic self-cleansing of pulmonary alveoli," Ann. Occup. Hyg. **37**, 347 (1993).
[3] F. F. Espinosa and R. D. Kamm, "Thin layer flows due to surface tension gradients over a membrane undergoing non-uniform, periodic strain," Ann. Biomed. Eng. **25**, 913 (1997).
[4] D. Zelig and S. Haber, "Hydrodynamics cleansing of pulmonary alveoli," SIAM (Soc. Ind. Appl. Math.) J. Numer. Anal. **63**, 195 (2003).
[5] H.-H. Wei, S. W. Beninitendi, D. Halpern, and J. B. Grotberg, "Cycle-induced flow and transport in a model of alveolar liquid lining," J. Fluid Mech. **483**, 1 (2003).
[6] H. Wong, D. Rumschitzki, and C. Maldarelli, "Marangoni effects on the motion of an expanding or contracting bubble pinned at a submerged tube tip," J. Fluid Mech. **379**, 279 (1999).
[7] M. R. Davidson and J. M. Fitz-Gerald, "Flow patterns in models of small airway units of the lung," J. Fluid Mech. **52**, 161 (1972).
[8] S. Haber, J. P. Butler, H. Brenner, I. Emanuel, and A. Tsuda, "Shear flow over a self-similar expanding pulmonary alveolus during rhythmical breathing," J. Fluid Mech. **405**, 243 (2000).
[9] H. Wong, D. Rumschitzki, and C. Maldarelli, "On the surfactant mass balance at a deforming fluid interface," Phys. Fluids **8**, 3203 (1996).
[10] J. Happel and H. Brenner, *Low Reynolds Number Hydrodynamics* (Prentice Hall, Englewood Cliffs, NJ, 1983).
[11] N. J. DeMestre and D. C. Guiney, "Low Reynolds number oscillatory flow through a hole in a wall," J. Fluid Mech. **47**, 657 (1971).
[12] G. Green, "Solution of some problems in viscous flow," Philos. Mag. **35**, 250 (1944).
[13] J. Ferziger and M. Peric, *Computational Methods for Fluid Dynamics* (Springer, Berlin 2002).
[14] C.-M. Lim, Y. Koh, T. S. Shim, S. D. Lee, W. S. Kim, D. S. Kim, and W. D. Kim, "The effect of varying inspiratory to expiratory ratio on gas exchange in partial liquid ventilation," Chest **116**, 1032 (1999).
[15] A. Podgorski and L. Gradon, "Dynamics of pulmonary surfactant system and its role in alveolar cleansing," Ann. Occup. Hyg. **34**, 137 (1990).
[16] M. K. White and D. S. Strayer, "Survival signaling in type II pneumocytes activated by surfactant protein-A," Exp. Cell Res. **280**, 270 (2002).